doi: 10.1115/ICEF2019-7169 Pre-Print

Proceedings of the ASME 2019 Internal Combustion Engine Division Fall Technical Conference
ICEF2019
October 20-23, 2019, Chicago, IL, USA

EFFECT OF HYDROGEN AND CARBON MONOXIDE ADDITION TO METHANE ON LAMINAR BURNING VELOCITY

Mohammadrasool Morovatiyan
Dept. of Mechanical Engineering
University of Massachusetts Lowell
Lowell, MA, USA

Martia Shahsavan
Dept. of Mechanical Engineering
University of Massachusetts Lowell
Lowell, MA, USA

Mammadbaghir Baghirzade
Dept. of Mechanical Engineering
University of Massachusetts Lowell
Lowell, MA, USA

J. Hunter Mack
Dept. of Mechanical Engineering
University of Massachusetts Lowell
Lowell, MA, USA

ABSTRACT

Exhaust gas recirculation (EGR) in spark-ignited engines is a key technique to reduce in-cylinder NOx production by decreasing the combustion temperature. The major species of the exhaust gas in rich combustion of natural gas are hydrogen and carbon monoxide, which can subsequently be recirculated to the cylinders using EGR. In this study, the effect of hydrogen and carbon monoxide addition to methane on laminar burning velocity and flame morphological structure is investigated. Due to the broad flammability limit and high burning velocity of hydrogen compared to methane, this addition to the gaseous mixture leads to an increase in burning velocity, less emissions production, and a boost to the thermal efficiency of internal combustion engines. Premixed CH_4-H_2-CO-Air flames are experimentally investigated using an optically accessible constant volume combustion chamber (CVCC) accompanied with a high-speed Z-type Schlieren imaging system. Furthermore, a numerical code is applied to quantify the laminar burning velocity based on the pressure rise during flame propagation within the CVCC. According to the empirical and numerical results, the addition of hydrogen and carbon monoxide enhances laminar burning velocity while influencing the flame structure and development.

KEYWORDS

Constant Volume Combustion Chamber, Premixed Combustion, Exhaust Gas Recirculation, Laminar Burning Velocity, Flammability Limit, Natural Gas, Syngas

1. INTRODUCTION

The use of exhaust gas recirculation (EGR) in spark-ignited (SI) engines effectively reduces in-cylinder NOx emissions through a reduction of the combustion temperature [1-5]. Moreover, employing high levels of EGR (EGR percentage > 15%) has the potential of increasing the fuel efficiency [2], reducing knock [6-9], and reducing the emissions of CO [7] and particulate matter [10, 11]. Dedicated EGR (D-EGR) is an SI engine concept that reforms the fuel composition and is capable of providing elevated EGR levels [12]. The D-EGR concept suggests a new configuration for operating engine cylinders, in that at least one cylinder is allocated to operate in fuel-rich combustion and to recirculate the resultant exhaust gases to the remaining cylinders, working in fuel-lean combustion. Rich combustion of natural gas in the dedicated cylinder delivers elevated levels of hydrogen and carbon monoxide. According to a previous study [13], 10-15% H_2 enrichment has been predicted using the D-EGR approach; the operation potentially increases the flame burning velocity and enhances engine stability [14-16]. Additionally, it has been assumed that whatever CO_2 and H_2O present from the D-EGR cylinder will be removed before recirculating the gases. Figure 1 shows a schematic diagram of a boosted spark-ignited engine with D-EGR.

Laminar burning velocity is a classical property in spark-ignited premixed combustion that aids in understanding reactivity, diffusivity, and exothermicity of a mixture [17-20]. Turbulent combustion models use this phenomenon to investigate turbulent flame development, emissions formation, flame structure, and instability. By employing laminar burning velocity to a proposed

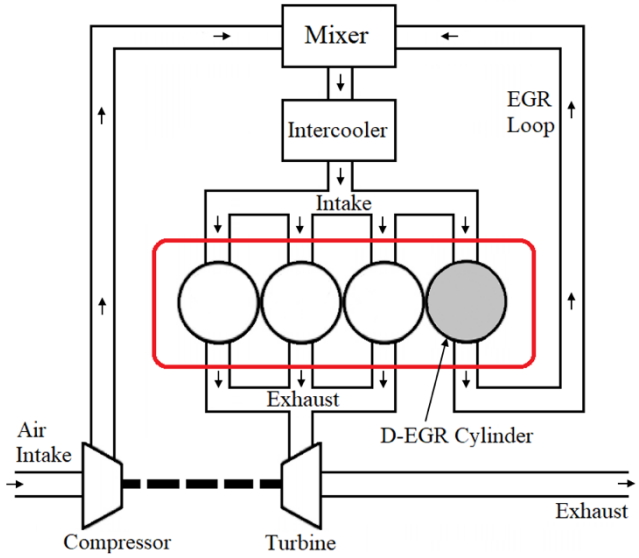

Figure 1. Schematic diagram of the D-EGR engine approach.

turbulent model, Keck [21] examined turbulent flame speed and flame structure in spark-ignited internal combustion engines. In order to study the instability and wrinkling in turbulent combustion, Menon et al suggested a turbulent combustion model that employed laminar burning velocity [22]. Another turbulent model was experimentally studied to anticipate flame stretch by using laminar burning velocity [23]. Additionally, the laminar burning velocity can be used for validating chemical kinetic models [24, 25].

In this study, the effect of hydrogen and carbon monoxide addition to methane on laminar burning velocity, flame morphological structure, and instability in an optically accessible constant volume combustion chamber is examined. It is assumed that rich natural gas combustion in a D-EGR cylinder produces the elevated levels of hydrogen and carbon monoxide. A synthetic fuel (syngas) with a ratio of 1:1 for these two species is used, and the mixture is added to methane. In this experiment, the laminar burning velocity of spherically expanding premixed CH_4-H_2-CO-Air flames is quantified for different syngas volumetric compositions (0-20% for H_2 and 0-20% for CO) in methane-syngas mixture at a wide range of equivalence ratios (0.5-1.4), an initial pressure of 1 bar, and an initial temperature of 298 K. Adding syngas to methane shows a positive dependency on the laminar burning velocity while extending the lower/upper flammability limits. Furthermore, the flame morphological structure and instability of CH_4-H_2-CO-Air combustion have been examined during flame development through the CVCC.

2. METHODS

2.1 Experimental Facilities

A 1.93 liter stainless steel constant volume combustion chamber (CVCC) is utilized to investigate the spherically expanding

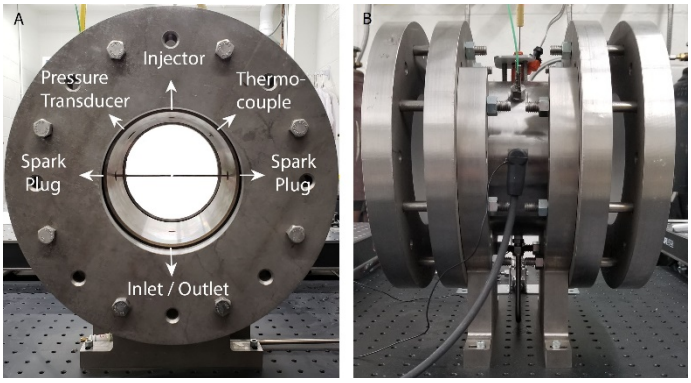

Figure 2. Optical cylindrical constant volume combustion chamber in (A) Side view, (B) Front view.

flame propagation, flame morphological structure, and instability [26]. The CVCC is equipped with two 50.8 mm thick flat quartz windows to visually provide side access into the chamber and observe the combustion process. The optically accessible CVCC is sealed with four elastomer O-rings mounted between the windows and the flanges. In order to measure the pressure trace during the combustion, a Kistler 601CAA high precision piezoelectric pressure transducer is connected to a Kistler 5018B charge amplifier. An Omega KMTXL-062G-6 thermocouple is mounted on the chamber to measure the initial temperature of the mixture. To generate a flame and initiate a combustion event, an ignition system including an ignition coil and two 2.5 mm thick extended spark plugs has been used to trigger a spark by spark plugs. The spark plugs are symmetrically installed on both sides to provide a central spark gap of 1.2 mm. A GM LS1/LS6 ignition coil is employed to provide a maximum voltage of 38 kV and a maximum discharge energy of 84 mJ. Figure 2 indicates the optically accessible constant volume combustion chamber with the instruments installed.

In order to examine flame development and instability, a high-speed CMOS camera (Edgertronic SC2+) is employed in a Z-shape Schlieren system. This optical system also includes a light source, a condensing lens, a pinhole, two concave mirrors with a focal length of 152.4 mm and an internal diameter of 152.4 mm, and a knife edge. The camera image capture rate is up to 31,191 frames per second with an exposure rate from 1/30 to 1/800,000 second that are optimized based on flame speed and image brightness, respectively. The light beams are emitted from a light source and passed through a condensing lens and a pinhole prior to reaching the first mirror. The beams are parallelly reflected through the chamber from the first mirror to the second mirror, and finally collected at the knife edge and reach the CMOS camera. The pinhole and the knife edge should be placed in the focal length of the mirrors to properly collect the beams and reflect them in the Schlieren imaging system.

To supply the desired gases to the optically accessible chamber, a gas delivery system is employed with a pressure control unit and four high accuracy pressure transducers operating at

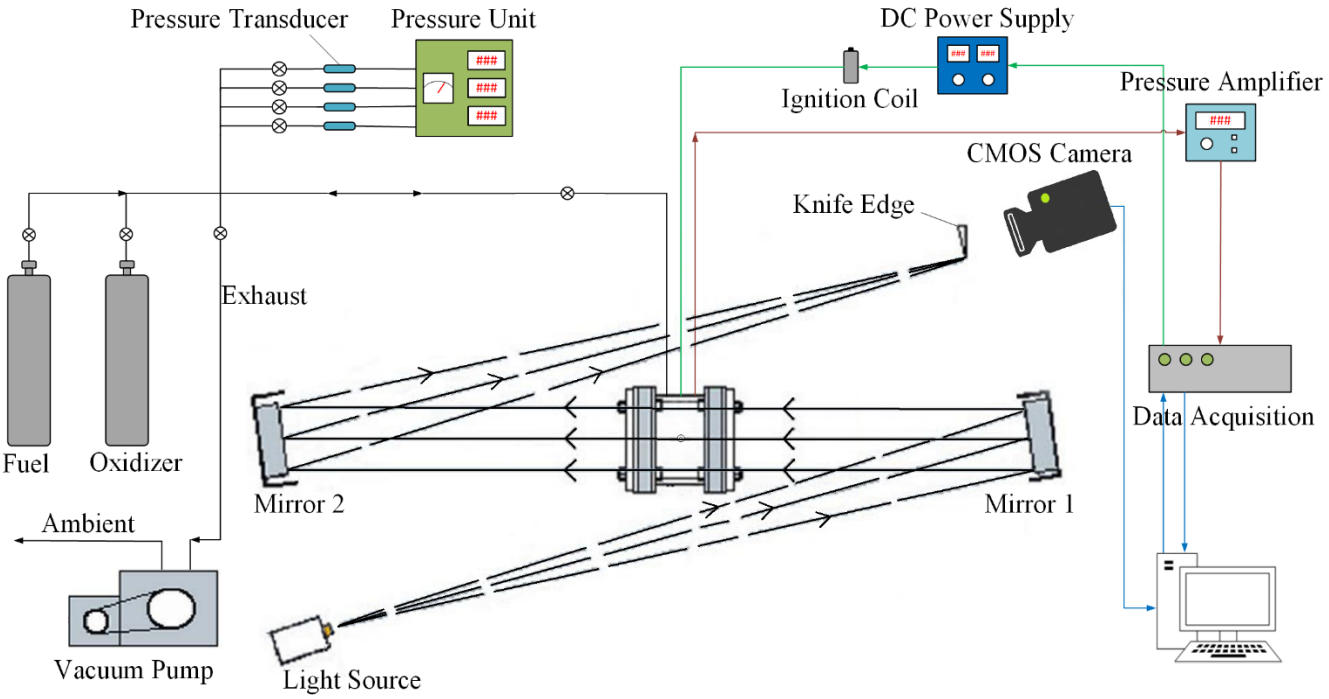

Figure 3. Schematic diagram of the experimental system including gas supply system and electrical controlling units.

different ranges. In order to collect the pressure and temperature data, a data acquisition system and LabVIEW software are connected to the electrical apparatus including the camera, the ignition system, the pressure transducer, and thermocouple. Figure 3 shows the schematic diagram of the experimental setup.

2.2 Experimental Procedures

The filling process of the optical CVCC is started with vacuuming the chamber and the gas supply system to empty the vessel of any residual gas that can impact subsequent results. According to the desired mixture, the chamber is then filled with partial pressures of gases in ascending order. In order to calculate the partial pressure of each gas, a MATLAB script is developed based on the ideal gas law and atomic balance applied on the global chemical reaction of the mixture. The gas supply system is vacuumed after filling the CVCC with each gas to ensure the line is empty of the previous gas and ready for the next gas. The desired mixture in the chamber is given 5 minutes to reach steady state. This is enough time to produce a homogenous, quiescent mixture with uniform temperature. By triggering a spark in the center of the chamber, the flame kernel is initiated and a thin flame sheet is spherically propagated through the vessel. According to a statistical study, each empirical condition was repeated at least three times to reach a confidence level of greater than 95% [27].

2.3 Laminar Burning Velocity Measurement

Laminar burning velocity is calculated based on a numerical model that uses experimental pressure-time data during the combustion process in the CVCC as an input. Due to this, the pressure-time data is first evaluated for a region that flame propagates laminar, smooth, and unstretched. According to previous studies on cylindrical constant volume combustion chambers [28], the flame front shows high stretch rates from the flame kernel initiation to the area that flame radii are less than 4 cm. Therefore, the lower margin of the pressure-time data that can be utilized for calculation of laminar burning velocity is started from this flame radius to the chamber radius to ensure the flame front is unstretched with negligible thickness. Moreover, by reaching the chamber wall, the flame front starts to wrinkle and becomes instable. Due to the energy loss of the burned gases, a negative effect on the pressure rise is observed that determines the upper margin of the pressure-time data. Another effective factor that limits the upper margin is instability. Any cellular flame formation is considered as an unsmooth non-laminar flame propagation that updates the upper margin. Additionally, the buoyancy effects in the combustible mixture are hydrodynamic-driven instability that should be considered. In order to study the flame structure and instability, an optically accessible cylindrical constant volume combustion chamber with an accurate optical diagnostic is required. This limited range of the pressure-time data is employed to measure the laminar burning velocity of premixed flames.

In this study, the initial mixture components for spherically expanding premixed CH_4-CO-H_2-Air flames are assumed as demonstrated below (where α = 0-20%):

$$\varphi\left((1-2\alpha)\,CH_4+\alpha\,H_2+\,\alpha\,CO\right)+\frac{1}{2}(\,O_2+3.76N_2) \quad (1)$$

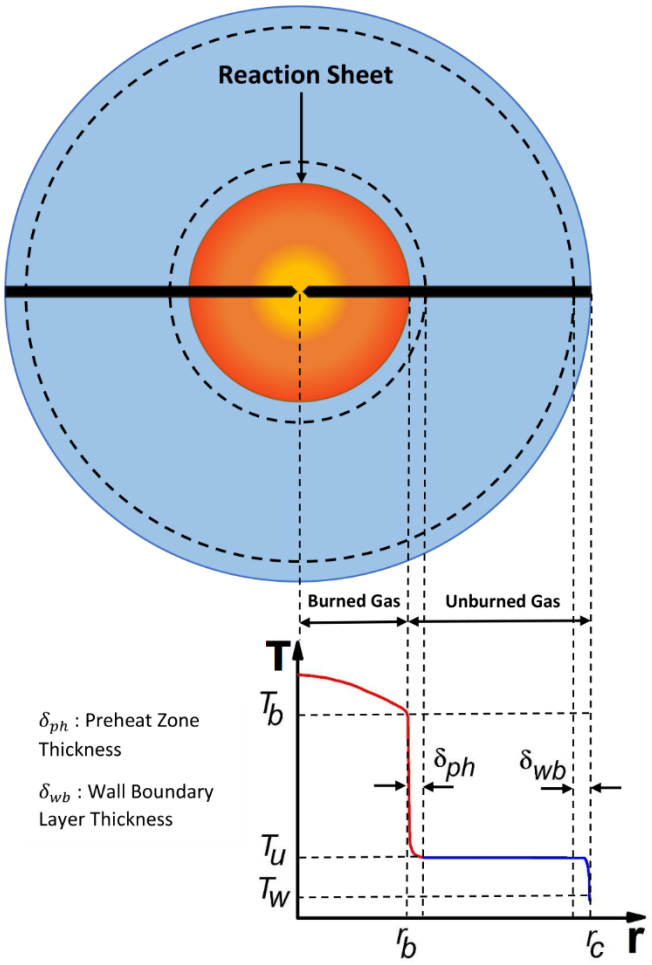

Figure 4. Schematic of the multi-shell thermodynamic model.

In order to calculate the laminar burning velocity, a thermodynamic multi-shell numerical model is developed based on a fundamental study conducted by Metghalchi-Keck [29]. This model introduces a displacement thickness concept and converts experimental dynamic pressure data to laminar burning velocity. It is primarily assumed that the flame is expanded spherical and smooth, and divides a closed CVCC into two specific regions of burned and unburned gases separated by a flame sheet with a negligible thickness (shown schematically in Figure 4). Furthermore, this model assumes that the burned and unburned gases are considered as an ideal gas and compressed isentropically. The burned gases are in the chemical equilibrium state with a negligible thermal gradient. The core unburned gas region is separated from the burned gas region and the chamber wall by a preheat zone (with a negligible thickness of δ_{ph}) and a thermal boundary layer (with a thickness of δ_{wb}), respectively. The pressure distribution through the chamber is assumed spatially uniform.

By applying conservation of mass and volume on the spherically expanding premixed flame in the closed chamber and using the ideal gas assumption, the total mass and volume including burned and unburned gases are defined as follows:

$$m_i = m_b + m_u = P_i(V_b + V_u)/RT_i \tag{2}$$

$$V_i = \int_0^{m_b} v_b dm + \int_{m_b}^{m_i} v_u dm \tag{3}$$

where m, V, and v are the mass, volume, and specific volume of the gas mixture, respectively. P and T represent pressure and temperature distribution through the chamber with the specific gas constant of R. The subscript of i refers to the initial conditions, while subscripts of b and u denote the burned and unburned gas regions.

The second term of Equation 2 related to the unburned gas region includes two specific parts: first, a part that unburned gases and the chamber wall are divided by the thermal boundary layer, and second, the core unburned gas region that is far from this boundary layer with a uniform temperature distribution and compressed isentropically. The superscript ∞ denotes the second part.

$$\int_{m_b}^{m_i} v_u dm = \frac{R}{P}\int_{m_b}^{m_i} (T_u - T^{\infty})dm + \int_{m_b}^{m_i} v_u^{\infty} dm \tag{4}$$

Equations 3 and 4 are combined by describing a concept of displacement thickness (δ) as shown below, where ρ and A are a density of a specific region and combustion chamber wall area, respectively.

$$\delta = \frac{1}{\rho^{\infty}}\int_0^{\infty} (\rho_u - \rho^{\infty})\, dr \tag{5}$$

$$V_i + A\delta = \int_0^{m_b} v_b dm + \int_{m_b}^{m_i} v_u^{\infty} dm \tag{6}$$

By dividing this equation by m_i and changing the infinitesimal mass coordinate, Equation 6 is revised as:

$$\frac{V_i}{m_i} + \frac{A\delta}{m_i} = \int_0^{x} v_b dx' + \int_x^{1} v_u^{\infty} dx' \tag{7}$$

where x refers to the mass fraction of the burned gas region and x' is an integration variable.

The energy balance equation applied to the gaseous mixture within the closed chamber is represented in the following equation for both burned and unburned gas regions where E_i and Q are total initial energy and total energy transferred to the chamber wall, respectively.

$$E_i - Q = \int_0^{m_b} e_b\, dm + \int_{m_b}^{m_i} e_u\, dm \tag{8}$$

The second term of Equation 8 is derived with two specific parts (indicated in Equation 9) since the unburned gas region contains

two parts. In this equation, C_v is constant volume specific heat of the unburned gases.

$$\int_{m_b}^{m_i} e_u \, dm = C_v \int_{m_b}^{m_i} (T_u - T^{\infty}) \, dm + \int_{m_b}^{m_i} e_u^{\infty} \, dm \qquad (9)$$

By assuming a 1-D heat conduction equation for heat transfer at the chamber wall, and changing the infinitesimal mass coordinate, and dividing by m_i, Equation 8 is described as below:

$$\frac{E_i}{m_i} - \frac{A}{m_i} \int_0^{\infty} P \, d\delta' = \int_0^{x} e_b \, dx' + \int_x^{1} e_u^{\infty} \, dx' \qquad (10)$$

The mass fraction and temperature of the burned gases are calculated by simultaneously solving both non-linear Equations of 7 and 10. The laminar burning velocity of the spherically expanding flame is finally computed by:

$$S_u = \dot{m}_b / \rho_u^{\infty} A_b = m \dot{x}_b / \rho_u^{\infty} A_b \qquad (11)$$

where $\dot{m}_b$ is mass burning rate and $\dot{x}_b$ is the rate of mass fraction burned.

The burned gases properties at the local chemical equilibrium states during flame propagation are calculated by coupling the CANTERA (an open-source chemical kinetic code) [30] with the numerical model. The JANAF thermodynamical tables are employed to compute the thermodynamic properties of the unburned gases [31].

3. RESULTS AND DISCUSSION

3.1 Flame Morphological Structures

Figure 5 illustrates the flame snapshots of the premixed CH_4-H_2-CO-Air flames for different compositions of hydrogen and carbon monoxide in the mixture at equivalence ratios of 0.5, 0.6 and 1.4, an initial pressure of 1 bar, an initial temperature of 298K, and at a flame radius of 55 mm. According to these images, the effect of adding syngas to methane is significant that extends lower and upper flammability limits of the methane. At equivalence ratios of 0.5 and 1.4 which are lower and upper margins of flammability limit of methane combustion, respectively, 0% to 10% addition for each H_2 and CO species is not sufficient to combust the mixture; however, adding 20% H_2 and 20% CO effectively enriches the mixture to initiate a flame. This range is extended due to the broad flammability limit of hydrogen that has been become dominant in the mixture.

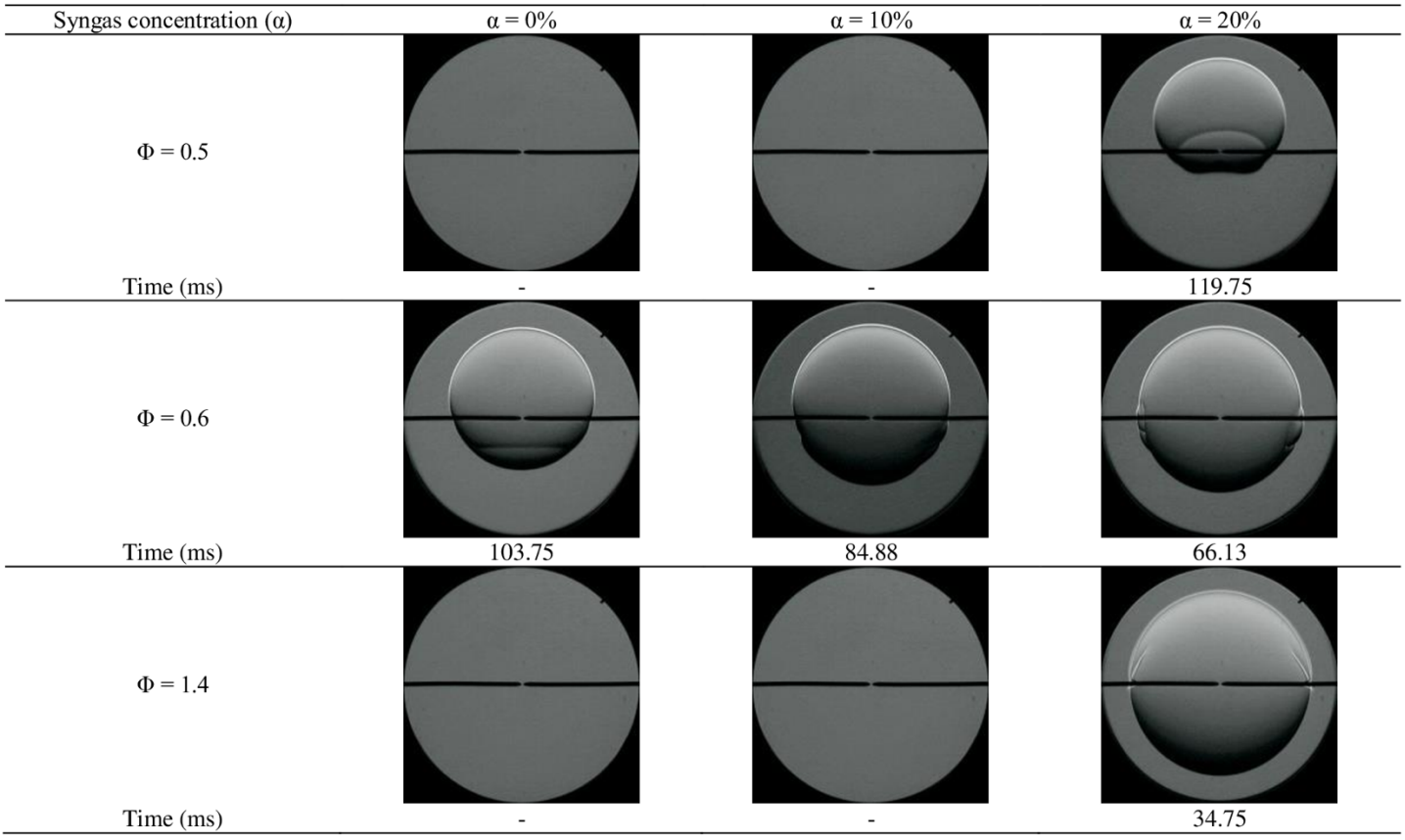

Figure 5. Snapshots of premixed CH_4-H_2-CO-Air flames at an initial pressure of 1 bar and an initial temperature of 298 K at flame radius of 55 mm.

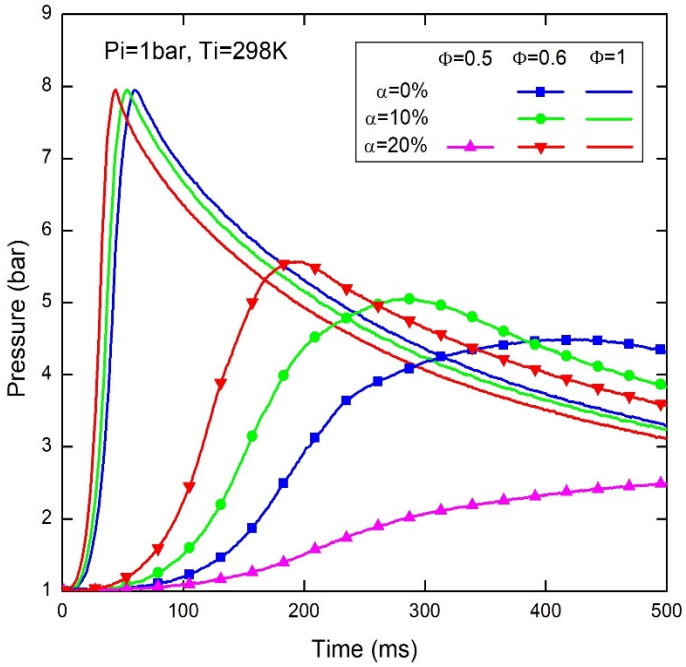

Figure 6. Pressure history of premixed CH_4-H_2-CO-Air combustion for three different syngas percentages and three equivalence ratios at an initial pressure of 1 bar and an initial temperature of 298 K.

Moreover, although this syngas addition leads to a flame propagation, it is not expanded symmetrical towards the chamber wall and buoyancy effect appears at equivalence ratios of 0.5 and 0.6. At these two equivalence ratios, the flame propagation rates are very slow that causes a buoyant flame and shifts the flame development towards the top portion of the chamber. This buoyancy effect is due to a density variation across the flame front. According to Figure 6 that shows pressure history at these two equivalence ratios, the pressure rises very slow; however, the temperature increases very fast and reaches a high flame temperature. Based on the ideal gas law, density is directly proportional to pressure and inversely to temperature. At the closed vessel, this causes a high density difference across the flame front between the burned and unburned gas regions. Due to very slow flame propagation and the high density variation at Φ=0.5 and 0.6, the flame is not able to overcome the buoyancy as a gravity force and thus hydrodynamic instability becomes significant. In other equivalence ratios, flame fronts are spherically expanded.

The flame development images of premixed CH_4-H_2-CO-Air flames for different flame radii at two equivalence ratios of 0.6 and 1, an initial pressure of 1 bar, and an initial temperature of 298K are shown in Figure 8. Although flames are propagated spherical and smooth, flame cracks are observed in some images. This is only due to the effect of the spark plug extended electrodes and is not associated with any type of instabilities.

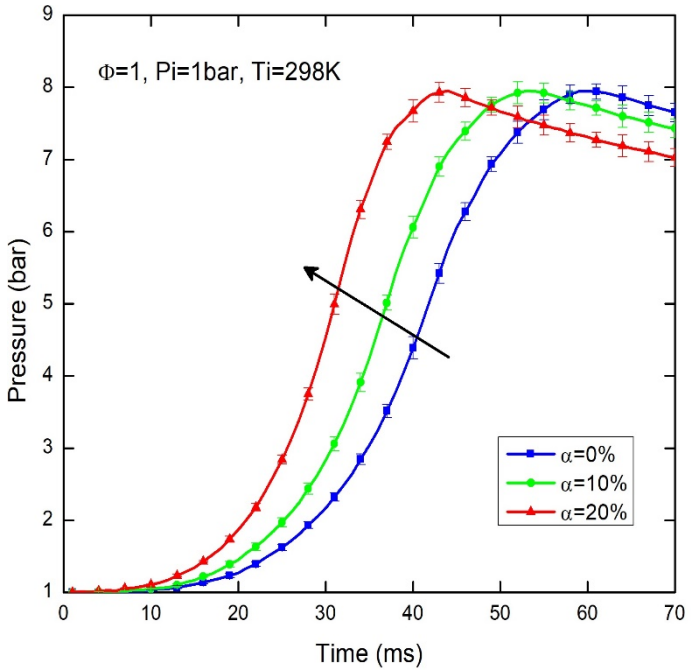

Figure 7. Pressure history of premixed CH_4-H_2-CO-Air combustion for three different syngas percentages at stoichiometric condition, an initial pressure of 1 bar, and an initial temperature of 298 K.

3.2 Pressure

The experimental pressure history of premixed CH_4-H_2-CO-Air combustion at equivalence ratios of 0.5, 0.6, and 1 for three different syngas additions at an initial pressure of 1 bar and an initial temperature of 298 K is illustrated in Figure 6. A sharp rise in pressure data implicitly indicates a swift burning flame front, while a very slow pressure rise demonstrates a very slow flame propagation rate that drives the flame front towards quenching at the top portion of the chamber. At Φ=0.5 and α=20%, the pressure increases very slow that indicates a buoyant rise. This buoyancy is also observed at Φ=0.6 for all cases. Furthermore, at both equivalence ratios of 0.6 and 1, adding syngas to methane yields a higher peak pressure that happens quicker; however, at Φ=1, peak pressures for all cases do not show a significant difference. In order to carefully examine syngas addition at Φ=1, Figure 7 displays the pressure rises in a shorter time duration. As syngas addition increases, its effect on pressure rise becomes more meaningful. Compared to α=0 and 10%, the pressure increases quicker at α=20% that implies a higher flame propagation rate. This may be explained as a higher fuel enrichment by increasing hydrogen concentration in the mixture.

3.3 Burning Velocity

Figure 9 plots the effect of equivalence ratio on the laminar burning velocity of CH_4-H_2-CO-Air flames for three different syngas volumetric additions to methane. In all cases, a negative

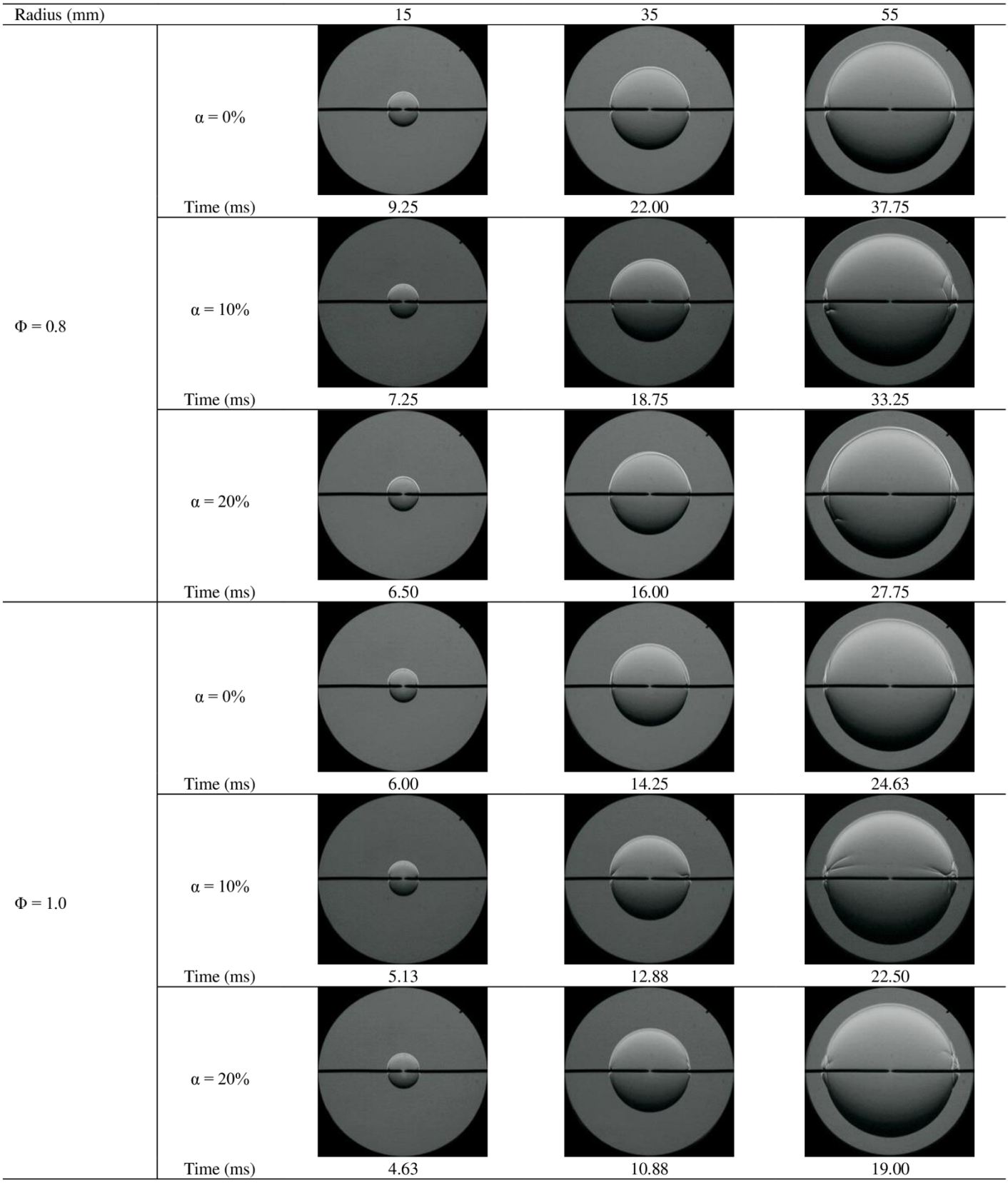

Figure 8. Snapshots of premixed CH_4-H_2-CO-Air flames for different syngas additions at an initial pressure of 1 bar and an initial temperature of 298 K at different flame radii

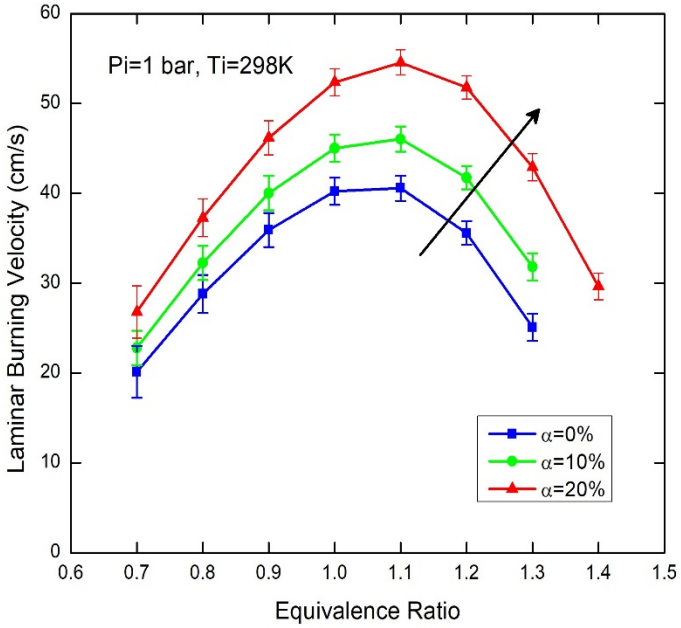

Figure 9. Effect of equivalence ratio on laminar burning velocity of CH_4-H_2-CO-Air combustion for different syngas additions to methane at an initial pressure of 1 bar and an initial temperature of 298 K.

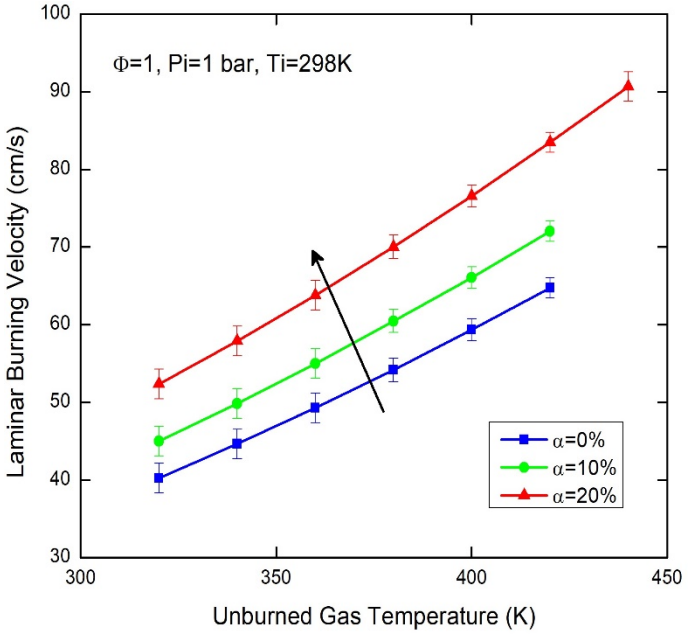

Figure 10. Effect of unburned gas temperature on laminar burning velocity of premixed CH_4-H_2-CO-Air combustion for different syngas additions to methane at an initial pressure of 1 bar and an initial temperature of 298 K.

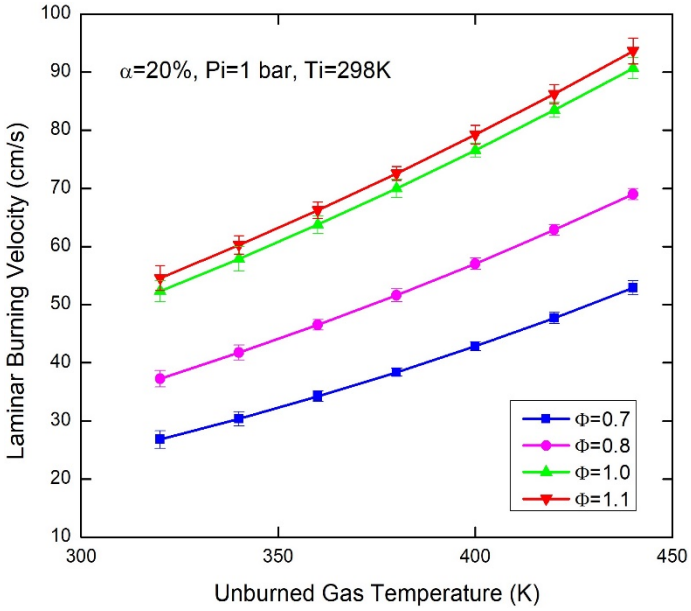

Figure 11. Effect of unburned gas temperature on laminar burning velocity of CH_4-H_2-CO-Air combustion for α=20% at different equivalence ratios, an initial pressure of 1 bar, and an initial temperature of 298 K.

parabolic behavior for laminar burning velocity in terms of equivalence ratio is observed. Increasing equivalence ratio leads to an increase and subsequent a decrease at adiabatic flame temperature. Due to this temperature variation, the unburned density first decreases and then increases by increasing equivalence ratios. According to Equation 11, since the unburned density inversely relates to the laminar burning velocity, this parabolic behavior is explained. Moreover, the effect of the highest syngas addition (α=20%) to methane shows a higher growth in laminar burning velocity at rich conditions compared to lean conditions. As the equivalence ratio increases, the effect of hydrogen in the syngas addition becomes more dominant. According to earlier studies [18], the maximum laminar burning velocity of hydrogen-air combustion happens at an equivalence ratio of roughly 1.8. This implicitly means that hydrogen in the current mixture still tends to increase the laminar burning velocity of the flame front. However, since the major component of the fuel mixture in all cases is methane, the range of flammability limit does not heavily change and the effect of this addition is only shown with higher growth in laminar burning velocity at richer conditions. Although this effect is also observed at α=10%, it is not quite significant.

In Figure 10, the effect of unburned gas temperature on the laminar burning velocity of CH_4-H_2-CO-Air flames for three syngas additions to methane is presented. A positive dependency of unburned gas temperature on laminar burning velocity is clearly observed in all conditions [17, 32]. Furthermore, adding syngas to methane demonstrates a positive correlation on laminar burning velocity; however, this behavior at higher unburned gas temperatures becomes more significant. As discussed, hydrogen fuel in the mixture is a governing factor on increasing laminar burning velocity. Due to this, laminar burning velocity has a higher growth rate at α=20% than that of at α=10%. In order to examine the growth rate at α=20% in terms

of equivalence ratio, the effect of unburned gas temperature on laminar burning velocity for varied equivalence ratios is illustrated in Figure 11.

4. CONCLUSIONS

The effect of adding different compositions of hydrogen and carbon monoxide to methane in an optically accessible constant volume combustion chamber has been investigated. In addition, the laminar burning velocity and the flammability limit of premixed CH_4-H_2-CO-Air flames have been examined. This study serves the following outcomes:

- Fuel enrichment of methane with 20% syngas volumetric addition (20% H_2 and 20% CO) extends lower and upper flammability limits of methane at equivalence ratios of 0.5 and 1.4.
- The mixture with 0% and 10% syngas addition could not be ignited at the lower and upper margins of the flammability limit.
- Lean combustion of CH_4-H_2-CO-Air mixture at an equivalence ratio of 0.5 and 0.6 indicates the buoyant rise in the closed vessel as a result of the density variation across the flame front. Due to the hydrodynamic instability appearance, the experimental data collected for these conditions were not used for numerical data interpretation.
- The syngas addition to methane yields a positive dependency on the laminar burning velocity.
- At richer conditions, 20% syngas addition effectively makes the effect of hydrogen in the mixture dominant and leads to a higher growth in laminar burning velocity. This effect is not quite significant at leaner conditions and lower syngas additions.
- The higher syngas additions in the mixture increase luminosity of premixed flame due to the higher hydrogen concentration.

NOMENCLATURE

α	Hydrogen and carbon monoxide composition in fuel
δ	Displacement thickness
δ'	Integration variable
δ_{ph}	Preheat zone thickness
δ_{wb}	Wall boundary layer thickness
v_b	Specific volume of burned gases
v_u	Specific volume of unburned gases
v_u^∞	Specific volume of unburned gas that is compressed isentropically
ρ_u	Density of unburned gas within the thermal boundary layer
ρ^∞	Density of unburned gas that is compressed isentropically
φ	Equivalence ratio
A	Wall area of the CVCC
C_v	Specific heat capacity at constant volume
e	Specific internal energy
E_i	Total initial energy
m_b	Mass of burned gases
m_i	Total initial mass of the gaseous mixture
m_u	Mass of unburned gases
P_i	Initial pressure within the chamber
P	Pressure
Q	Total energy conducted from the flame to the wall
r	Radius of the CVCC
R	Specific gas constant
S_u	Laminar burning velocity
T_i	Initial temperature of the gaseous mixture
T_u	Unburned gas temperature within the thermal boundary layer
T^∞	Temperature of unburned gas that is compressed isentropically
V	Volume
x	Mass fraction of the burned gas

ACKNOWLEDGEMENTS

The authors would like to recognize the University of Massachusetts Lowell for supporting this research.

REFERENCES

[1] D. Pierpont, D. Montgomery, and R. D. Reitz, "Reducing particulate and NOx using multiple injections and EGR in a DI diesel," *SAE transactions,* pp. 171-183, 1995.

[2] M. Tabata, T. Yamamoto, and T. Fukube, "Improving NOx and fuel economy for mixture injected SI engine with EGR," *SAE transactions,* pp. 1221-1230, 1995.

[3] S. Szwaja, E. Ansari, S. Rao, M. Szwaja, K. Grab-Rogalinski, J. D. Naber, and M. Pyrc, "Influence of exhaust residuals on combustion phases, exhaust toxic emission and fuel consumption from a natural gas fueled spark-ignition engine," *Energy Conversion and Management,* vol. 165, pp. 440-446, 2018.

[4] M. R. Morovatiyan and V. Hosseini, "Development of a 3D CFD model to analyze gas exchange process into intake manifold of an iVVT engine," *The Journal of Engine Research,* vol. 36, no. 36, pp. 51-60, 2014.

[5] M. Darzi, D. Johnson, R. M. B. Bade, C. Ulishney, N. Zamani, N. Clark, G. Thompson, and P. Famouri, "Continuously Varying Exhaust Outlet Diameter to Improve Efficiency and Emissions of a Small SI Natural Gas Two-Stroke Engine by Internal EGR," SAE Technical Paper0148-7191, 2018.

[6] B. Grandin, H.-E. Ångström, P. Stålhammar, and E. Olofsson, "Knock suppression in a turbocharged SI engine by using cooled EGR," SAE Technical Paper0148-7191, 1998.

[7] T. Alger, T. Chauvet, and Z. Dimitrova, "Synergies between high EGR operation and GDI systems," *SAE International Journal of Engines,* vol. 1, no. 1, pp. 101-114, 2009.

[8] Y. Duchaussoy, A. Lefebvre, and R. Bonetto, "Dilution interest on turbocharged SI engine combustion," SAE Technical Paper0148-7191, 2003.

[9] A. Cairns, H. Blaxill, and G. Irlam, "Exhaust gas recirculation for improved part and full load fuel economy in a turbocharged gasoline engine," SAE Technical Paper0148-7191, 2006.

[10] M. Hedge, P. Weber, J. Gingrich, T. Alger, and I. Khalek, "Effect of EGR on Particle Emissions from a GDI Engine," *SAE International Journal of Engines,* vol. 4, no. 1, pp. 650-666, 2011.

[11] T. Alger, J. Gingrich, I. A. Khalek, and B. Mangold, "The role of EGR in PM emissions from gasoline engines," *SAE International Journal of Fuels and Lubricants,* vol. 3, no. 1, pp. 85-98, 2010.

[12] C. Chadwell, T. Alger, J. Zuehl, and R. Gukelberger, "A demonstration of dedicated EGR on a 2.0 L GDI engine," *SAE International Journal of Engines,* vol. 7, no. 1, pp. 434-447, 2014.

[13] E. Randolph, R. Gukelberger, T. Alger, T. Briggs, C. Chadwell, and A. Bosquez Jr, "Methanol fuel testing on port fuel injected internal-only EGR, HPL-EGR and D-EGR® engine configurations," *SAE International Journal of Fuels and Lubricants,* vol. 10, no. 3, pp. 718-727, 2017.

[14] T. D'Andrea, P. Henshaw, and D.-K. Ting, "The addition of hydrogen to a gasoline-fuelled SI engine," *International journal of hydrogen energy,* vol. 29, no. 14, pp. 1541-1552, 2004.

[15] J. A. Goldwitz, "Combustion optimization in a hydrogen-enhanced lean burn SI engine," Massachusetts Institute of Technology, 2004.

[16] M. D. Gerty and J. B. Heywood, "An investigation of gasoline engine knock limited performance and the effects of hydrogen enhancement," SAE Technical Paper0148-7191, 2006.

[17] O. Askari, Z. Wang, K. Vien, M. Sirio, and H. Metghalchi, "On the flame stability and laminar burning speeds of syngas/O2/He premixed flame," *Fuel,* vol. 190, pp. 90-103, 2017.

[18] M. Morovatiyan, M. Shahsavan, J. Aguilar, and J. H. Mack, "The Effect of Working Fluids on Premixed Hydrogen Combustion in a Constant Volume Combustion Chamber," *11th U. S. National Combustion Meeting,* March 24–27 2019.

[19] S. Zare, S. Roy, A. El Maadi, and O. Askari, "An investigation on laminar burning speed and flame structure of anisole-air mixture," *Fuel,* vol. 244, pp. 120-131, 2019.

[20] C. Xiouris, T. Ye, J. Jayachandran, and F. N. Egolfopoulos, "Laminar flame speeds under engine-relevant conditions: uncertainty quantification and minimization in spherically expanding flame experiments," *Combustion and Flame,* vol. 163, pp. 270-283, 2016.

[21] J. C. Keck, "Turbulent flame structure and speed in spark-ignition engines," in *Symposium (International) on Combustion*, 1982, vol. 19, no. 1, pp. 1451-1466: Elsevier.

[22] S. Menon and A. R. Kerstein, "Stochastic simulation of the structure and propagation rate of turbulent premixed flames," in *Symposium (International) on Combustion*, 1992, vol. 24, no. 1, pp. 443-450: Elsevier.

[23] S. Shy, P. Ronney, S. Buckley, and V. Yakhot, "Experimental simulation of premixed turbulent combustion using aqueous autocatalytic reactions," in *Symposium (International) on Combustion*, 1992, vol. 24, no. 1, pp. 543-551: Elsevier.

[24] Y. Dong, A. T. Holley, M. G. Andac, F. N. Egolfopoulos, S. G. Davis, P. Middha, and H. Wang, "Extinction of premixed H2/air flames: Chemical kinetics and molecular diffusion effects," *Combustion and Flame,* vol. 142, no. 4, pp. 374-387, 2005.

[25] S. Dooley, M. P. Burke, M. Chaos, Y. Stein, F. L. Dryer, V. P. Zhukov, O. Finch, J. M. Simmie, and H. J. Curran, "Methyl formate oxidation: Speciation data, laminar burning velocities, ignition delay times, and a validated chemical kinetic model," *International journal of chemical kinetics,* vol. 42, no. 9, pp. 527-549, 2010.

[26] M. Morovatiyan, M. Shahsavan, M. Shen, and J. H. Mack, "Investigation of the Effect of Electrode Surface Roughness on Spark Ignition," in *ASME 2018 Internal Combustion Engine Division Fall Technical Conference*, San Diego, CA, 2018, no. 51982, p. V001T03A022, Volume 1: Large Bore Engines; Fuels; Advanced Combustion: American Society of Mechanical Engineers.

[27] W. M. Trochim and J. P. Donnelly, *Research methods knowledge base*. Atomic Dog Publishing Cincinnati, OH, 2001.

[28] Z. Chen, M. P. Burke, and Y. Ju, "Effects of compression and stretch on the determination of laminar flame speeds using propagating spherical flames," *Combustion Theory and modelling,* vol. 13, no. 2, pp. 343-364, 2009.

[29] M. Metghalchi and J. C. Keck, "Burning velocities of mixtures of air with methanol, isooctane, and indolene at high pressure and temperature," *Combustion and flame,* vol. 48, pp. 191-210, 1982.

[30] D. G. Goodwin, R. L. Speth, H. K. Moffat, and B. W. Weber, "Cantera: An object-oriented software toolkit for chemical kinetics, thermodynamics, and transport processes," Version 2.4.0 ed, 2018.

[31] J. Malcolm W. Chase, *NIST-JANAF Thermochemical Tables* (Washington, DC; New York :American Chemical Society; American Institute of Physics for the National Institute of Standards and Technology). 1998.

[32] Z. Wang, Z. Bai, G. Yu, S. Yelishala, and H. Metghalchi, "The Critical Pressure at the Onset of Flame Instability of Syngas/Air/Diluent Outwardly Expanding Flame at Different Initial Temperatures and Pressures," *Journal of Energy Resources Technology,* vol. 141, no. 8, p. 082207, 2019.